Climatic Change (2024) 177:107
https://doi.org/10.1007/s10584-024-03765-8

# Depth-dependent warming of the Gulf of Eilat (Aqaba)

**Sounav Sengupta**[1] · **Hezi Gildor**[2] · **Yosef Ashkenazy**[1]

Received: 12 December 2023 / Accepted: 12 June 2024 / Published online: 25 June 2024


**Abstract**
The Gulf of Eilat (Gulf of Aqaba) is a semi-enclosed basin situated at the northern end of the Red Sea, renowned for its exceptional marine ecosystem. To evaluate the response of the Gulf to climate variations, we analyzed various factors including temperature down to 700 m, surface air temperature, and heat fluxes. We find that the sea temperature is rising at all depths despite inconclusive trends in local atmospheric variables, including the surface air temperature. The Gulf's sea surface temperature (SST) warms at a rate of a few hundredths of a degree Celsius per year, which is comparable to the warming of the global SST and the Mediterranean Sea. The increase in sea warming is linked to fewer winter deep mixing events that used to occur more frequently in the past. Based on the analysis of the ocean-atmosphere heat fluxes, we conclude that the lateral advection of heat from the southern part of the Gulf likely leads to an increase in water temperature in the northern part of the Gulf. Our findings suggest that local ocean warming is not necessarily associated with local processes, but rather with the warming of other remote locations.

**Keywords** Gulf of Eilat (Gulf of Aqaba) · Climate change · Ocean warming · Heat fluxes

## 1 Introduction

The warming of sea and air temperatures in different parts of the world is well established. According to the recent Intergovernmental Panel on Climate Change (IPCC) [1] the Earth's oceans continue to warm due to human activity. It was reported that the ocean temperature has increased over the past few decades, absorbing more than 90% of the excess heat in the Earth's system. This increase in heat has caused the ocean to expand and contributed to ∼43% of observed global mean sea level rise between 1970 and 2015. Newer estimates of ocean heat uptake in the top 2000 m between 1993 and 2017 range from 9.2±2.3 ZJ/yr to 12.1±3.1 ZJ/yr [2]; 1 zettajoule (ZJ) equals $10^{21}$ J. The updated estimates for ocean heat uptake in the upper ocean (0-700 meters) indicate warming with more recent periods experiencing faster rates of warming. In addition, the rate of heat uptake for deeper layers has been higher in the last three decades [2].

✉ Sounav Sengupta
sounav.sengupta4@gmail.com

[1] Department of Environmental Physics, BIDR, Ben-Gurion University, Midreshet Ben-Gurion, Kibbutz, Israel

[2] The Institute of Earth Sciences, The Hebrew University of Jerusalem, Jerusalem, Israel

A warming trend in the global subsurface ocean has been identified, separate from natural variations. This warming pattern consists of three main components: long-term warming, El Niño/Southern Oscillation-related (ENSO) warming [3], and Atlantic Multidecadal Oscillation-related warming [4;5]. Long-term warming accounts for 78% of the global temperature variance down to 300 m depth [6]. In addition, the rate of increase in global average sea surface temperature (SST) is around 0.033°C/yr, based on data analyzed from 1982 to 2023 [7]. During this same period, the Mediterranean Sea has experienced an increase of around 0.036°C/yr [7;8].

Nisha et al. [3] examine a long-term trend and interannual variability of heat content down to 300 m of the Arabian Sea (2000-2017), attributing spring/summer warming to subsurface heat accumulation, and fall/winter to mixed layer heat. El Niño/Southern Oscillation (ENSO) and Indian Ocean Dipole (IOD) drive the interannual variability below the mixed layer, while advection and air-sea fluxes impact different seasons, emphasizing the role of these dynamics in marine heatwaves, cyclones, and regional climate predictions.

Narrowing down to the area of our study (Fig. 1), Chaidez et al. [9] analyzed the Red Sea's temperature patterns from 1982 to 2015, focusing on the SST maxima. The northern part of the Red Sea is warming faster than the southern part, exceeding the global warming rate with a warming trend of 0.40°C to 0.45°C per decade. The Red Sea overall is warming at a rate of $0.17 \pm 0.07$°C per decade.

The Gulf of Eilat (hereafter the "Gulf") hosts a diverse ecosystem, and it was suggested that the Gulf may be the last refuge for coral reefs [10]. Previous studies addressed the ocean warming's impact on the Gulf's ecosystem [11–13], where frequent events of coral bleaching and various forms of anthropogenic stresses influencing the ecosystem have been mentioned due to the rise in the ocean temperature. Here we investigate the presence of discernible trends within the temperature profiles of the water column within the Gulf. Our analysis reveals a rising temperature trend throughout the water column, a trend seemingly disconnected from immediate local atmospheric conditions. Instead, it appears to be intricately linked to the advection of water from southern latitudes, implying a plausible scenario of warming occurring within the Red Sea [14]. This horizontal advection of water from the Red Sea is confined by shallow sills and an upper warm layer of water with a weak vertical stratification [15;16;14;13;17]. Precisely estimating the heat and water exchange between the atmosphere and the ocean is crucial for gaining insights into thermoregulation mechanisms

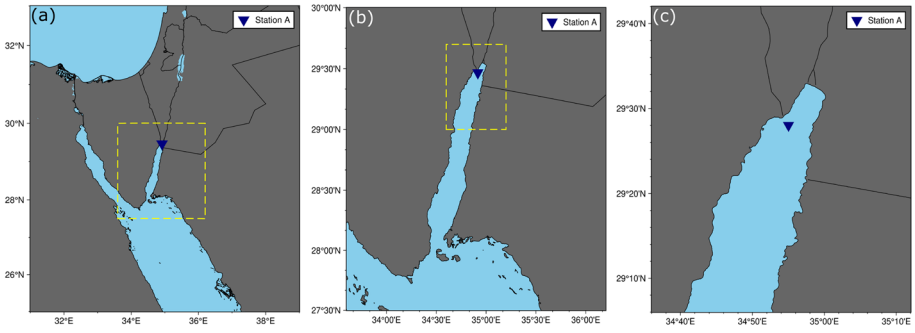


**Fig. 1** (a) An areal picture of the Red Sea. (b) The Gulf of Eilat blends into The Red Sea. (c) Location of Station A at which the oceanic data has been collected

and for developing accurate models of ocean dynamics [18]. Hence, a long-term analysis of sea and air temperature, like the analysis performed in this study, can facilitate a deeper understanding of the climate system and its effect on the marine ecosystem. A primary limitation of the study is the relatively short duration of both meteorological (16 years) and oceanic (20 years) observations. Additionally, the analysis is based on data from only one location (Station A), which may limit the generalizability of the findings.

The distinctive statistical methodology employed herein underscores the robustness of our conclusions regarding the substantive warming trends observed over the years of sampled data. Below we first provide a brief introduction to the Gulf (Section 2). Afterward, we describe the oceanic (Section 3.1) and meteorological (Section 3.2) datasets, and the methodology employed (Section 3.3). We then present the results that are based on oceanic data (Section 4.1) and meteorological data (Section 4.2), including the estimation of surface heat fluxes in the Gulf (Section 4.3). We discuss and conclude the study in Section 5.

## 2 The study area: the gulf of eilat (Aqaba)

The Gulf is situated at the northern tip of the Red Sea and is surrounded by the Sinai and the Arabian peninsula (Fig. 2). It is an elongated semi-enclosed basin that is approximately 180 km long, 5-25 km wide, and has a maximum depth of 1820 m. The Gulf is connected to the Red Sea through the Straits of Tiran (orange triangle in Fig. 2), which have a maximum depth of 245 m [15;19]. The Gulf abodes a diverse ecosystem of coral reefs and their associated fisheries, that are under the influence of significant anthropogenic stress [20;21;12;22].

The water column's temperature profile in the northern Gulf exhibits pronounced seasonal variations. During the summer and autumn seasons, from June to October, the upper mixed layer of the water column extends down to a depth of ∼40 m, with SST of around 27°C. Below this mixed layer lies a stratified thermocline, extending to a depth of approximately 200 m [16]. Progressing further downward is a deep, nearly uniform layer that extends to the seafloor (reaching depths of over 700 m at the specified measurement location) and maintains a temperature of just under 21°C (see Fig. 3).

In Fig. 3 we have plotted the potential temperature-depth profile versus time to portray the mixing events throughout the duration of the whole data. Potential temperature refers to the temperature that a parcel of water would attain under adiabatic conditions (i.e., no exchange of heat) as it is moved to a specified reference pressure (usually at the sea surface).

As the autumn season unfolds between October and December, the SST decreases due to atmospheric cooling. This cooling triggers, through vertical convection, a deepening of the mixed layer. Subsequently, during the winter season, from January to March, this vertical mixing process intensifies, causing the thermocline to largely dissipate. Consequently, a weak temperature contrast of less than 1°C prevails between surface water and deep water in most years; see Figs. 3, 4a. However, particularly cold years witness the complete erosion of the thermocline due to extensive deep mixing, resulting in the formation of a singular deep layer with uniform temperature and salinity [23;16;24] (see Fig. 3 and Fig. S1). A typical deep-mixing event exhibits a very negligible potential temperature difference throughout the mixed layer. Such complete mixing events were observed on the following dates: 20-03-2005, 12-03-2007, 12-02-2008, 13-03-2012, and 23-03-2022, indicating only one complete mixing event in the last 10 years; these are indicated by the arrows in Fig. 3 and in Fig. S2.

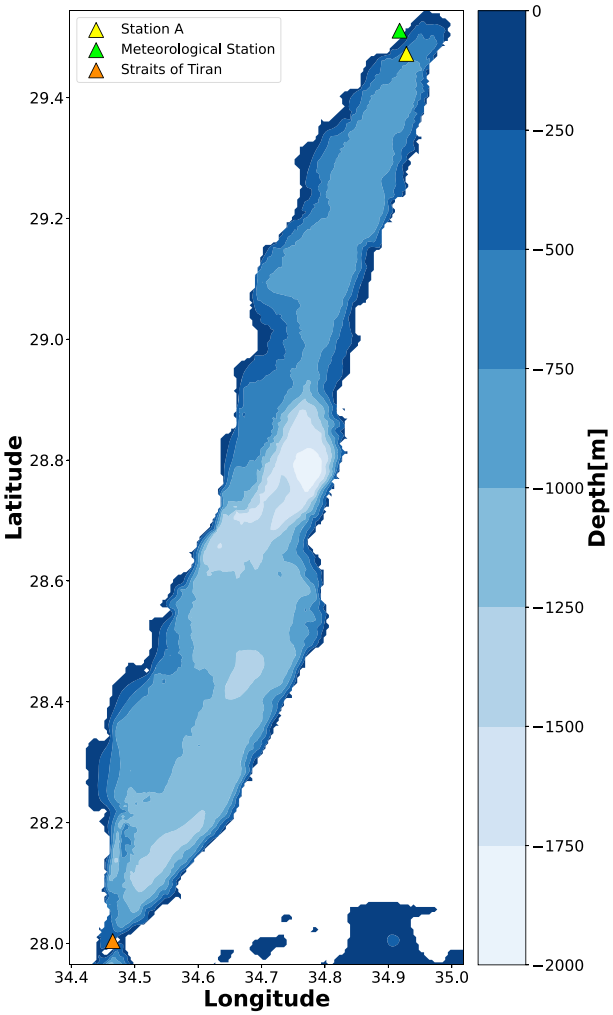


**Fig. 2** A depth contour map of the Gulf of Eilat and the locations of the oceanic Station A (yellow triangle), the meteorological station at the Inter-University Institute (green triangle), and the Straits of Tiran (orange triangle at the bottom)

The changes in the stratification of the Gulf across the seasons have significant impacts on both the Gulf's water dynamics and ecosystem. Seasonal changes influence the exchange flow with the Red Sea and the stratification in the Gulf [25]. The change in stratification also affects the magnitude of semi-diurnal tidal currents [26;27]. In winter, when the surface water is sufficiently cold and dense, deep mixing occurs, which permeates the deep waters and mixes nutrients into the photic zone. This nutrient enrichment triggers blooms of phytoplankton and zooplankton that peak at the beginning of the restratification phase, towards the end of the winter [28–30].

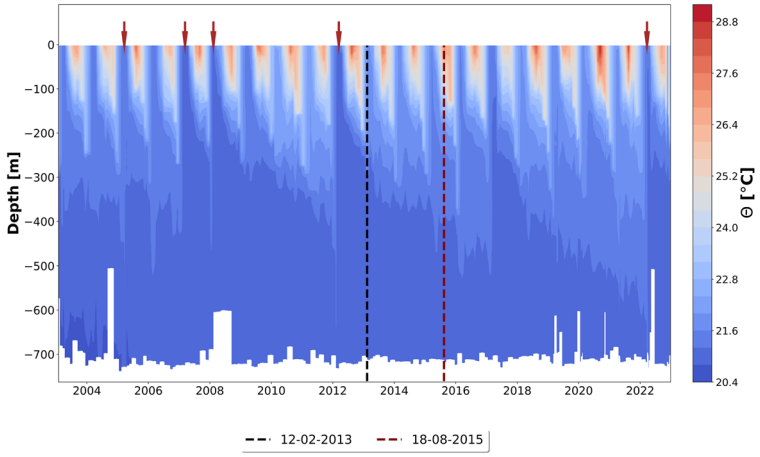


**Fig. 3** Water potential temperature (in °C) as a function of depth and time. The black and maroon vertical dashed lines indicate two specific dates whose potential temperature and salinity profiles are plotted in Fig. 4. The above measurements were collected every month at Station A in the northern part of the Gulf of Eilat (indicated by the yellow triangle in Fig. 2), between January 2003 and December 2022. The brown arrows signify each deep-mixing event throughout the time series (Fig. S2 shows potential temperature profiles of those events). The blank spaces at the bottom arise due to the variability of the maximum depth of each cast in the dataset

## 3 Data and methods

### 3.1 Ocean data

The ocean data consists of 270 standard CTD (Conductivity, Temperature, and Depth) casts measured in "Station A" (29°C 28' N, 34°C 55' E, indicated by the yellow triangle in Fig. 2).

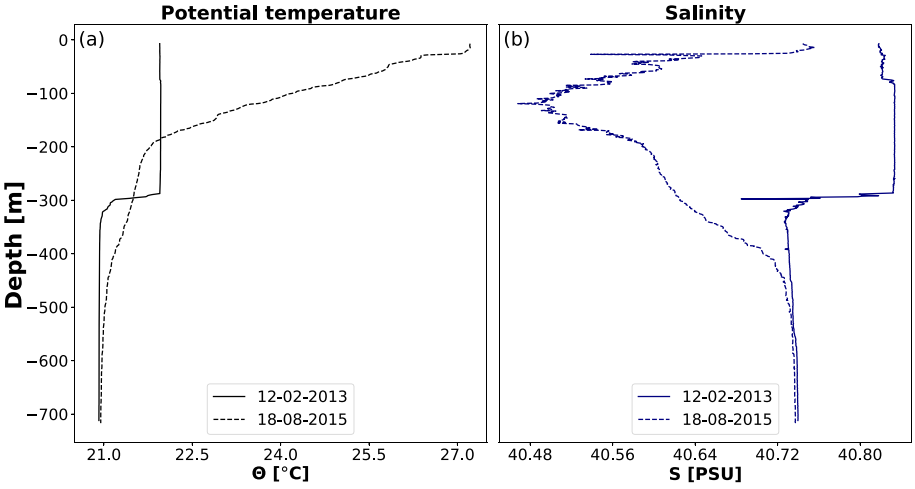


**Fig. 4** (a) Gulf potential temperature and, (b) salinity depth profiles at a typical winter month (12-02-2013) and a typical summer month (18-08-2015). These dates are marked by the black and maroon vertical dashed lines in Fig. 4

A CTD device is crucial for studying seawater properties. It consists of probes attached to a rosette wheel lowered into the ocean. Each cast includes measurements of pressure, in-situ temperature, conductivity, photosynthetic active radiation (PAR), and fluorescence. Some of these measurements are used to calculate the depth, salinity, and density. The different variables are collected in real time and transmitted to a shipboard computer. Sampling water at specific depths can help understand the physical properties of different locations over time. The data was collected on monthly cruises as part of the Israeli national ocean monitoring program. To study the deep water temperature temporal variations, we consider casts that extend to depths below 500 m. We binned the data into a one-meter resolution, to allow consistent statistical analysis. The ocean data (potential temperature and salinity) we analyze here is depicted in Fig. 3 and Fig. S1, consisting of typically 1 cast per month, from January 2003 to December 2022 (20 years). The maximum depth of these measurements is ∼750 m (see Fig. 2). We note that casts have been conducted at different phases of the tides which stimulate internal waves which can shift up and down the isotherms by a few tens of meters [31]. In Fig. S11 we show the temperature profiles of two typical casts at two different times of the day, where the shift in the isotherms is apparent. This is expected to increase the variability of the temperature at the thermocline, and hence to increase the uncertainty of our results. Despite this, we find a significant warming along the entire water column.

### 3.2 Meteorological data

The meteorological data has been recorded at the end of the dock of the Israeli Inter-University Institute (IUI) for Marine Sciences, Eilat (29°C30.211' E, 34°C 55.068' N, indicated by the green triangle in Fig. 2), where a comprehensive set of environmental parameters are being measured. The main mast, situated 10 m above sea level at low tide, serves as the reference point for recording wind speed, wind direction, air temperature, and relative humidity. Barometric pressure is measured 5 m above sea level, and adjustments are made to ensure sea level calibration. For capturing solar radiation data, a sensor is fixed on a cross-arm extending 0.7 m southward from the main mast, positioned 6 m above sea level.

The atmospheric data we analyzed span the period from the beginning of January 2007 to the end of December 2022 (16 years). The collected data included a 10-minute average of the different variables including (10 m) surface air temperature (SAT), SST (measured at a 2 m depth), sea level pressure, solar radiation, 10 m wind speed and direction, relative and absolute humidity, photosynthetic active radiation (PAR), and UV radiation. We constructed the daily and monthly averages of the data which have been used to calculate the heat fluxes and their climatological seasonal cycle.

### 3.3 Methods

#### 3.3.1 Ocean data analysis

In our study, we aim to investigate possible long-term temporal trends (i.e., beyond the seasonal cycle) in various environmental variables (including the SAT and various heat fluxes discussed below), with a particular focus on water temperature. To accomplish this, we employed the method of least square linear regression on data points (time series) binned at different depths. It is essential to emphasize that we do not assume the trends are linear; rather, we used linear regression solely to quantify the general increase or decrease of the different variables over the duration of the measurements.

To assess the significance of these trends, we implemented the following statistical approach. We conducted random shuffling of the time series for each variable (at each depth), a process we repeated many times (typically 1000 times). By shuffling the time series, we effectively destroy the temporal order and thereby render it random [32;33]. Consequently, any genuine temporal patterns (including trends) that might have existed in the original data were disrupted in the shuffling procedure. We then performed linear regression on each of the shuffled time series to calculate the slopes of their respective trends. The mean of these slopes should be around zero as there are no correlations in the shuffled time series. By constructing a Probability Density Function (PDF) of the slopes obtained from the shuffled time series, we generated an essential tool for evaluating the significance of the trend slopes observed in the original data. If the actual slope of the trend in the original time series lies well outside the confidence interval of the PDF generated from the shuffled slopes, it suggests that the observed trend is statistically significant, up to the confidence level. In other words, the probability of obtaining such a slope by random chance alone is exceedingly low, providing evidence for a meaningful temporal trend in the variable under consideration [34]. This methodology ensures that our conclusions regarding the significance of the observed trends are robust. The above procedure can be applied both for oceanic and meteorological data.

Both the different atmospheric and oceanic variables exhibit seasonal cycles that may make it difficult to estimate the temporal trends superimposed on the seasonal cycle. In light of the above, we have performed the estimations of the linear slope based on: (a) the original time series that includes the seasonal cycles, (b) the time series of a specific month (or season) over the years (e.g., considering the month of February of all years), and (c) on the anomalies around the seasonal cycle. It is clear that the uncertainty is the largest for (a); yet, for deep ocean measurements, the seasonal cycle is hardly present. We elaborate on the above below (Section 4.1).

#### 3.3.2 Meteorological data analysis

Our primary objective was to investigate long-term climate trends and understand the heat fluxes associated with the observed meteorological conditions. To achieve this, we computed the daily, monthly, and yearly averages for each of the atmospheric variables. This step allowed us to capture seasonal and annual variations in the meteorological parameters over the 16-year study period. Next, we employed bulk formulas to calculate the heat fluxes based on the derived averages.

#### 3.3.3 Heat flux analysis

The Gulf is connected to the Red Sea through the Straits of Tiran and the water exchange through the Straits affects the circulation and the structure of the water column in the Gulf [35; 36]. The energy balance in the Gulf is affected both by the local meteorological conditions and the water properties that are influenced by the water exchange through the straits of Tiran. The principle of energy conservation helps to understand the thermoregulation within a marine setting. The net heat flux, $Q$, of a water column can be formulated as follows [18;23]

$$\begin{aligned} Q &= \mathrm{SW} + \mathrm{LW} + \mathrm{LH} + \mathrm{SH} + \mathrm{ADV} \\ &= \mathrm{ASHF} + \mathrm{ADV}, \end{aligned} \tag{1}$$

where SW indicates the net (the incoming minus the reflected) shortwave (or solar) radiation, LW the net longwave radiation, LH the latent heat flux, SH the sensible heat flux, and ADV the heat transported by advection from the adjacent ocean. In our convention, positive fluxes are directed upward, while negative fluxes are directed downward, which explains the negative values of the SW radiation and the positive values of LW radiation respectively. The sum of the different components in Eq. 1 without the ADV term quantifies the net air-sea heat flux (ASHF) through the surface where positive values indicate that the water is losing heat (i.e., cooling down). The SW is directly measured while the other fluxes can be estimated using standard bulk formulas specified below [37]. Ideally, $Q$ should be zero and the ADV can be quantified accordingly. In this study, we do not explicitly calculate the ADV since our data is based on a single-point measurement.

The latent and sensible heat fluxes can be estimated [38–41] based on the wind speed and differences in humidity and temperature between the sea surface and the air surface:

$$\begin{aligned} \mathrm{LH} &= C_e \rho L \left(q_s - q_a\right) W, \\ \mathrm{SH} &= C_h \rho C_p \left(T_s - T_a\right) W, \end{aligned} \tag{2}$$

where $L$ denotes the latent heat constant of vaporization ($2.5 \times 10^6\ \mathrm{J\,kg^{-1}}$), $\rho$ is the air density ($1.2\ \mathrm{kg\,m^{-3}}$), $q_s$ and $q_a$ are the saturated specific humidity calculated using the SST ($T_s$ in °C) and surface air temperature ($T_a$ in °C), $W$ (in $\mathrm{m\,s^{-1}}$) is the wind speed, $C_e$ and $C_h$ are the moisture and heat transfer coefficients, and $C_p$ is the specific heat constant of air.

The longwave radiation (LW) has been parameterized previously based on the calculation of water vapor pressure and the atmospheric emissivity [42]. There are at least eight formulas that are used to calculate the longwave radiation, some of them incorporate a cloudiness factor for a more accurate estimation [43;44]. Here we use the formula of Berliand et al. (1952) [45] to estimate the LW; we chose a cloudiness factor of $c = 1$ since the Gulf has fairly clear sky conditions throughout the year:

$$\mathrm{LW} = -\epsilon\sigma T_a^4 (0.39 - 0.05\sqrt{e_a})c - 4\epsilon\sigma T_a^3 (T_s - T_a), \tag{3}$$

where $\epsilon (= 0.985)$ and $\sigma (= 5.6697 \times 10^{-8}\ \mathrm{Wm^{-2}K^{-4}})$ are the emissivity and Stefan-Boltzmann constants respectively. $T_s$ and $T_a$ are the SST and surface air temperature in K and $e_a$ is the water vapor pressure at a (2 m) standard height. During the summer season, the influence of the last term in Eq. 3 becomes dominant. This is due to the increased difference between the SST and the air temperature ($T_s - T_a$). The second term in Eq. 3 shows greater negativity, particularly in summer, due to warmer air temperatures compared to the cooler SST during this season. In contrast, the first term of Eq. 3 does not display a distinct seasonal pattern. Consequently, the combined effect of these two terms results in a minimal value for the outgoing LW in the summer months.

## 4 Results

### 4.1 Oceanic temporal trends and their significance

Figure 3 presents the potential temperature at Station A of the Gulf as a function of time and depth. The potential temperature profile shown in Fig. 3 exhibits a clear seasonal cycle with deep mixing of several hundred meters during the winter months (February and March) and a relatively shallow mixed layer of tens of meters during the summer (July and August) [31;46;47]. The difference in SST between the summer and winter is about 7°C and the mixed layer

is deepening towards the winter months when the SST becomes colder. Every few years, the ocean experiences a complete mixing down to almost to the bottom (see Fig. S2), while every year there is mixing to at least a few hundred meters; see Fig. 4a as an example. Below we show that deep mixing events become less frequent, leading to the warming of the entire water column in the Gulf.

The clear seasonal cycle observed in the water temperature is less apparent in the salinity field (Fig. S1) [48] [We note that the salinity data till 2010 may contain some inaccuracies related to the calibration of the CTD, which may affect the salinity results reported below.] Moreover, salinity profiles are not monotonic and there is a layer with a salinity minimum during the summer (e.g., Fig. 4b), due to the minimum in the salinity of the water entering through the Tiran Straits [25;9]. This is due to processes occurring in the Northern Red Sea which are beyond the scope of the paper. The salinity variations in the Gulf span 40.3 PSU to 40.8 PSU [28] while the temperature variations span 21°C to 28°C; simple analysis using a linear equation of state indicates that the density in the Gulf is temperature dominated [17]. This is further justified as follows: we estimated, based on the Gibbs-SeaWater (GSW) Oceanographic Toolbox (https://www.teos-10.org/pubs/gsw/html/gsw_contents.html), the thermal and haline expansion coefficients, $\alpha$ and $\beta$, for typical temperature (25°C) and salinity (41 PSU) values as $\alpha = 3.1 \times 10^{-4}$ °C$^{-1}$ and $\beta = 7.2 \times 10^{-4}$ PSU$^{-1}$. Thus, $\alpha \Delta T / \beta \Delta S \gtrsim 3$, indicating that the role of temperature variations on the density is more than 3 times larger than the contribution of the salinity. Following the above, and since the observed trend in the water is a warming trend, we mainly focus on the temperature variations.

To have a clear view of the structure of the water column, we show in Fig. 4 the potential temperature and salinity depth profiles in typical winter (12-02-2013) and summer (18-08-2015) dates; these are marked by the vertical black and maroon dashed lines in Fig. 3. The different water column layers are noticeable in the summer month temperature profile (Fig. 4a). The deep mixing of several hundred (∼300) meters is shown in (Fig. 4a,b).

We next analyze the temporal trends in oceanic temperature across the duration of the dataset. Fig. 5 depicts the water potential temperature and potential temperature anomalies as a function of time for distinct depth levels: shallow depths (20 m, Fig. 5a,d), intermediate depths (150 m, Fig. 5b,e), and deep ocean (600 m, Fig. 5c,f). Notably, the upper panels of

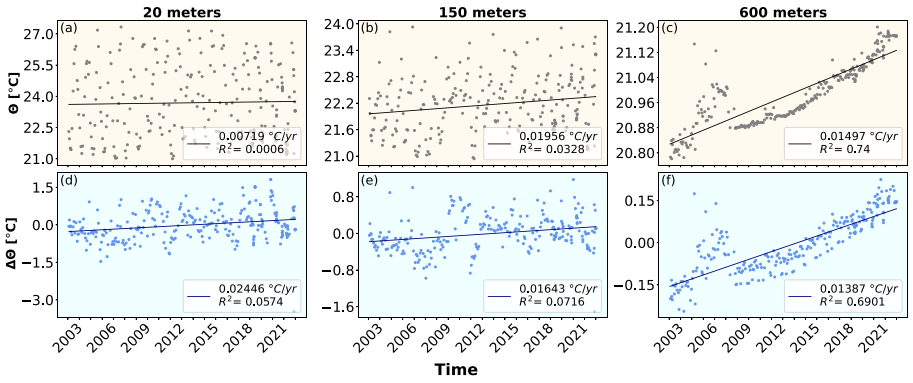


**Fig. 5** Water potential temperature and potential temperature anomaly as a function of time at depths of (a,d) 20 m, (b,e) 150 m, and (c,f) 600 m. The solid black lines indicate the linear regression where the slope is indicated in the lower right corner of each panel. The upper panels depict the original time series while the lower panels depict the anomaly time series after removing the seasonal cycle. Note the different scales of the y-axis in the different panels

Fig. 5 are augmented by linear regression lines, enabling the identification of nuanced trends within the dataset, often concealed by the dominant seasonal oscillations. It becomes evident that the temperature trends within the shallow and intermediate waters are considerably influenced by the seasonal cycle. However, a distinctive narrative unfolds within the deep ocean regions, where the influence of seasonal variability is notably diminished. Here, a discernible and statistically significant warming trend emerges. This trend is characterized by an annual temperature increase of approximately 0.015 $^{\circ}C\,yr^{-1}$.

To filter out the effect of the seasonal cycle, we have estimated the temporal trends in the ocean temperature after removing the seasonal cycle from the time series shown in Fig. 5a-c. To obtain the anomaly data, we subtracted the monthly mean from all the data points for each specific depth. The results are plotted in Fig. 5d-f, indicating clearer increasing trends in ocean temperature. We verify the significance of these trends below. The increase in water temperature range from $\sim$0.015 $^{\circ}C\,yr^{-1}$ at deep water, to $\sim$0.019 $^{\circ}C\,yr^{-1}$ at depth of 150 m, to $\sim$0.007 $^{\circ}C\,yr^{-1}$ at shallow water of 20 m.

To estimate the significance of the temperature trends (like the ones shown in Fig. 5), we conducted the hypothesis test described above in the Section 3.3.1 for each depth's temperature time series—the results revealed statistically significant increasing warming trends. Shortly, we shuffled each of the time series under consideration, typically 1000 times, and calculated their slopes. The PDF of the slopes of the shuffled time series should be centered around zero where the spread of the PDF of the slopes may provide a measure for the uncertainty of the observed slope.

Figure. 6a shows the PDF of the slopes of the shuffled time series of the depth of 150 m; the red point denotes the slope of the regression line of the original time series (shown in Fig. 5b). The slope of the original time series lays well outside the main part of the PDF of the slopes of the shuffled time series, indicating that the observed slope is significant. We have repeated the above procedure for all depths and present the results in Fig. 6d. Here, the slope of the original time series is indicated by the solid black line while the shading represents the 25%–75% confidence interval of the shuffled time series. The increasing trend in water temperature is highly significant except for the upper 50 m or so.

Furthermore, to account for seasonal variations explicitly, we segregated the data into winter (January to March) and summer (June to August) months and performed the shuffling test to determine the significance of the trends (see Fig. 6b,c). As expected, the increasing warming slopes are higher across all depths when considering separately the winter and summer months and these slopes are highly significant (Fig. 6e,f). Analysis of each month separately yielded similar results (Supplementary Fig. S4).

We repeated the above analysis on the anomaly time series of all the months and segregated summer and winter months, similar to Fig. 6d-f. In Fig. 6g-h the blue line indicates the slope of the regression of the original anomaly time series and the shaded region indicates the 25%–75% confidence interval of the PDF of the slopes of the shuffled anomaly time series. Almost all slopes of regression of the un-shuffled time series displayed in Fig. 6 are positive and highly significant, confirming a consistent temperature rise across all depths.

In addition to the above shuffling test, we performed a "weaker" shuffling procedure in which the order of the time series within each year remains unchanged where only the order of the different years was chosen randomly (Supplementary Fig. S5). The shuffling resulted in the identification of a significant water-warming trend.

In summary, we find that the water column in the Gulf exhibits a significant warming trend. A trend analysis of the salinity time series resulted in much weaker trends in the upper part of the water column and significantly increasing trends in the deep ocean; see Supplementary Figs. S6, S7.

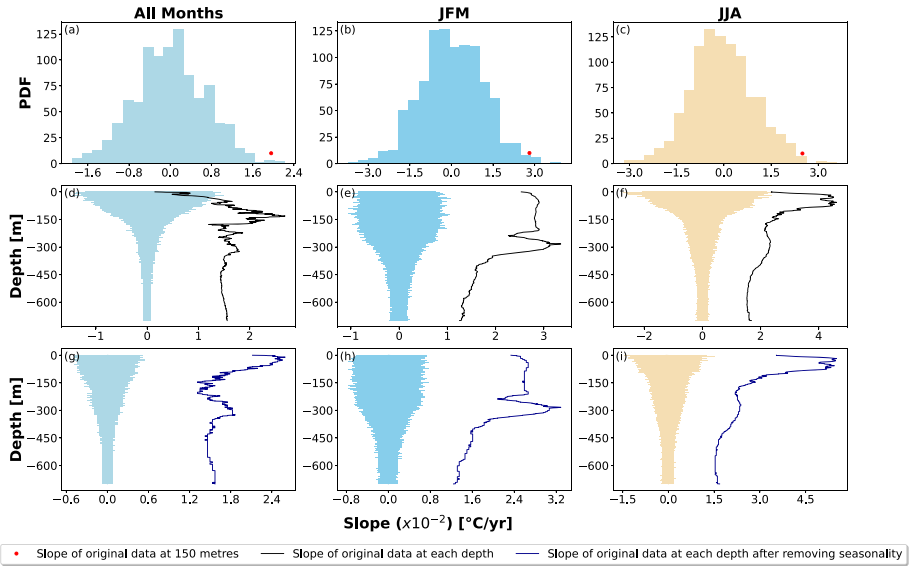


**Fig. 6** PDF of the slopes of the shuffled time series of 150 m depth for (a) the complete time series (shown in Fig. 4b), (b) of the winter months (January, February, and March stacked together), and (c) of the summer months (June, July, and August stacked together). The red dot in panels a-c indicates the slope of the original time series. The slope of the regression of the original time series versus depth (black line, in $^{\circ}$C yr$^{-1}$) and the 25%–75% confidence interval (light blue shading) of the slopes of the shuffled time series versus depth based on the (d) original time series (e) the stacked data of the winter months (JFM) and, (f) the stacked data of the summer months (JJA). (g), (h), (i) Same as d-f but for the anomaly time series where the slope of regression line is represented by the blue line

## 4.2 Meteorological data results

The meteorological data analysis is conducted using 10-minute averages of different variables, such as SAT and SST. Additionally, we examined the daily (24-hour) maximum and minimum SAT and SST. We also constructed the anomaly time series of the daily maximum and minimum time series of surface air temperature and SST (Fig. 7) and performed the trend analysis. We find that there is a significant increasing trend in the maximum and minimum SST (Fig. 8c,d); similar to the above, the analysis was based on the slopes of linear regression of 1000 shuffled time series. The SAT time series do not exhibit a similar increasing warming trend (Fig. 8a,b). The absence of trends in the SAT time series in contrast to the significant warming trends in the SST time series suggests that the local air temperature does not underlie the observed water warming. In addition to this analysis, we conducted the "weaker" shuffling procedure in which the order of the time series within each year remains unchanged where only the order of the different years was chosen randomly (Supplementary Fig. S8) and found similar results of an increasing warming trend in the SST time series but not in the surface air temperature time series.

Following the above, we adopted a different approach to studying possible temporal trends in surface air temperature and SST. The idea is to quantify the number of extreme cooling events and extreme warming events in the temperature time series; a reduction in extreme cooling events indicates a reduction in deep mixing events of the water column and hence

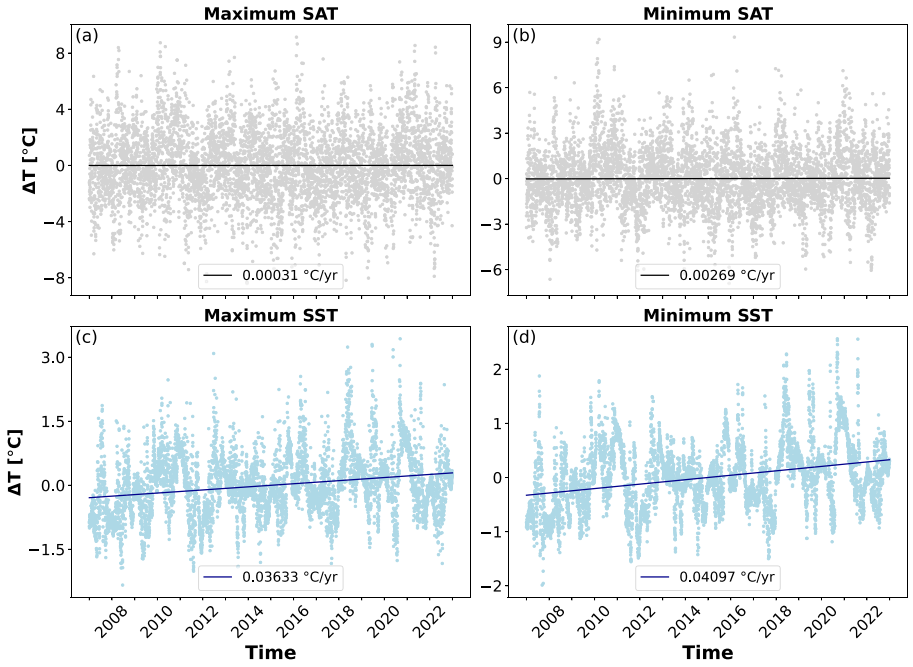


**Fig. 7** Anomaly time series of (a) daily maximum SAT, (b) daily minimum SAT, (c) daily maximum SST, and (d) daily minimum SST. The corresponding original time series are shown in Fig. S9

warming of the entire water column. Based on the 10-minute data we counted the number of times the temperature dropped below a certain threshold and exceeded a certain temperature threshold. The results are presented in Fig. 9 where it is apparent that while the analysis for the SAT (Fig. 9a,c) does not yield noticeable trends, these of the SST exhibit a general increase in the number of warming events (Fig. 9b) and reduced number of cooling events (Fig. 9d). A noticeable exception is the warming event of 2010 that yielded a reduced number of cooling events both in the SAT and SST (Fig. 9c,d). The above analysis is another indication of the warming of the Gulf's water. Yet, the absence of similar trends (or lack of correlations) in the SAT counts (Fig. 9a,c) suggests that changes in the SAT are not the primary cause for the warming of the water in the Gulf.

In light of the findings detailed above, it is necessary to consider other factors that can influence the SAT and SST differently. Local oceanographic processes, such as heat exchange with the atmosphere and coastal currents, can play a crucial role in modulating SST trends. Additionally, oceanic circulation may also lead to decoupling between the local atmospheric and oceanic temperature variations. These are described in more detail below.

Our findings are consistent with earlier research that has identified unique patterns for air temperature and SST in different geographical areas [49;50]. The decoupling of air temperature and SST trends can have implications for the local climate and marine ecosystems. Further investigations into the underlying mechanisms driving these trends are essential for gaining a comprehensive understanding of the climate dynamics in the Gulf area. To gain a deeper understanding of the process that causes the observed warming, we next examine the heat fluxes between the air and the sea.

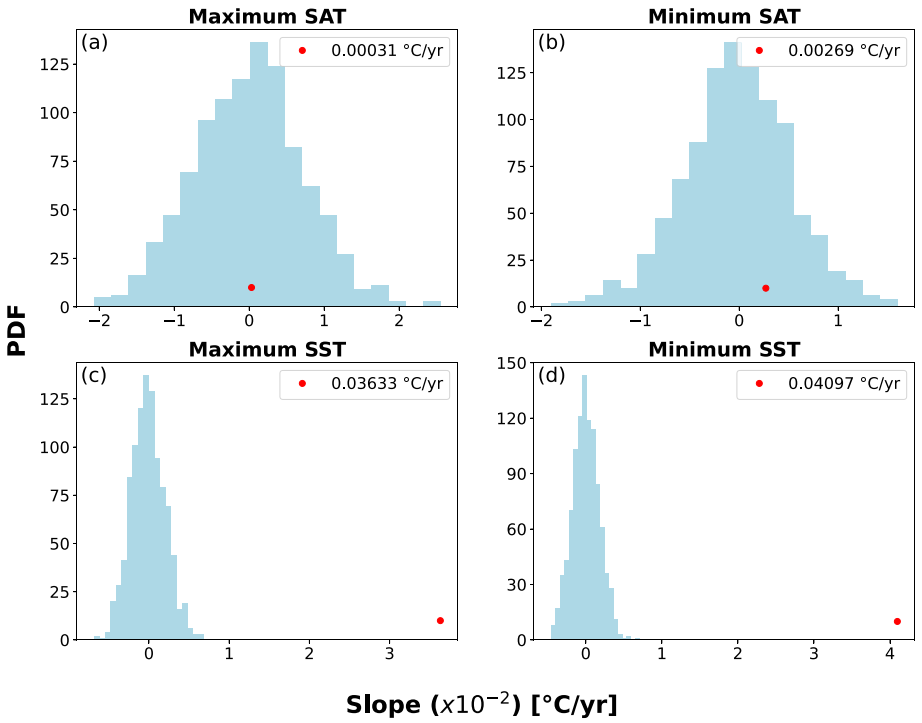


**Fig. 8** The PDF of the slopes of the shuffled time series of (a) daily maximum SAT, (b) daily minimum SAT, (c) daily maximum SST, and (d) daily minimum SST. The red dot indicates the slope of a linear regression performed on the original time series. Note the significant trend for the SST time series and the absence of trends for the SAT time series

### 4.3 Heat flux results

We calculated the different air-sea heat fluxes using the bulk formulas described in Section 3.3.3; an exception is the net shortwave radiation (SW), which was directly measured. We constructed the climatological seasonal cycle of the latent heat (LH), sensible heat (SH), SW, and longwave (LW) radiation; see Fig. 10 for the mean ± std seasonal cycle of the different fluxes. The LH is always positive as it is proportional to the difference between the saturated humidity at the sea surface to the actual humidity of the surface air—the saturated humidity is larger than the actual humidity. On the other hand, the SH is only positive during the winter months because it is constructed from the difference in SST and SAT; during the winter the air temperature can be lower than the SST while the opposite occurs during the summer (see Fig. S9).

The results described above are in general agreement with the results of Ben-Sasson et al. [23] who used one-year data of ocean temperature up to a depth of 750 m as well as meteorological data to analyze the Gulf's heat balance using specific bulk formulas, revealing insights into the heat flux and evaporation processes in the Gulf. Our analysis is based on a much longer time series of 16 years. The net heat flux shown in Fig. 10e is positive throughout the year such that the annual mean of the net heat flux is not zero as one would expect. This finding is similar to the results reported by Ben Sasson et al. [23] and suggests that warm water masses originating from the southern parts of the Gulf and the Red Sea contribute to the

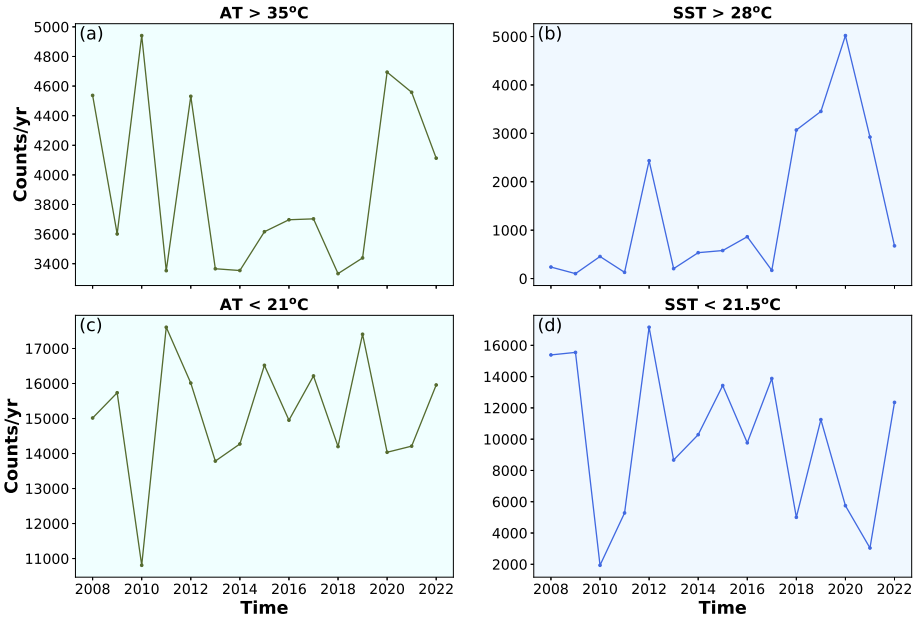


**Fig. 9** Counts (per year) of SAT (a) above 35°C and (c) below 21°C. Counts (per year) of SST (b) above 28°C and (d) below 21.5°C. The counts are based on the 10-minute time series which consists of 52560 data points per year

observed temperature changes in the Gulf and close the energy budget. Figure. 10 provides further insights into the seasonal variations in the average latent heat (LH). Interestingly, we observed a distinct peak in LH over the summer months, in contrast to Ben Sasson et al. [23]; this discrepancy may originate in the much shorter time series analyzed by Ben Sasson et al. [23].

The estimation of the heat fluxes is based on measured variables that include instrumental error. These include wind speed, SAT and SST, relative humidity, and global radiation. The accuracy of the measurement of wind speed is $\pm 0.3\ \mathrm{m\,s^{-1}}$ or 1% of the reading. For air temperature, the accuracy at 20°C is ±0.2°C. The accuracy of relative humidity at 20°C (field-calibrated against references) is ±2% for 0% to 90% of RH and ±3% for 90% to 100% of RH. For water temperature, the tolerance level of the probe is ±0.2°C over the 0°C to 70°Crange. The static accuracy of the instrument for water pressure is ±0.05% over a 0°C to 50°C temperature range. Finally, the sensitivity of the instrument for solar radiation is 7 to 14 $\mu\mathrm{V\,W^{-1}\,m^{-2}}$ with a temperature dependence on the sensitivity below 1%. Given the uncertainties in the measurement of the atmospheric parameters being relatively small, we can deduce that the uncertainty in the values of the heat fluxes calculated using bulk formulas is also low. Prior to the calculation, we filtered out the outliers which could affect the estimation of the heat fluxes.

## 5 Summary and conclusion

The multi-depth analysis of ocean temperature in our study has revealed a prominent and consistent warming in the past 20 years or so, resulting in less frequent deep mixing events.

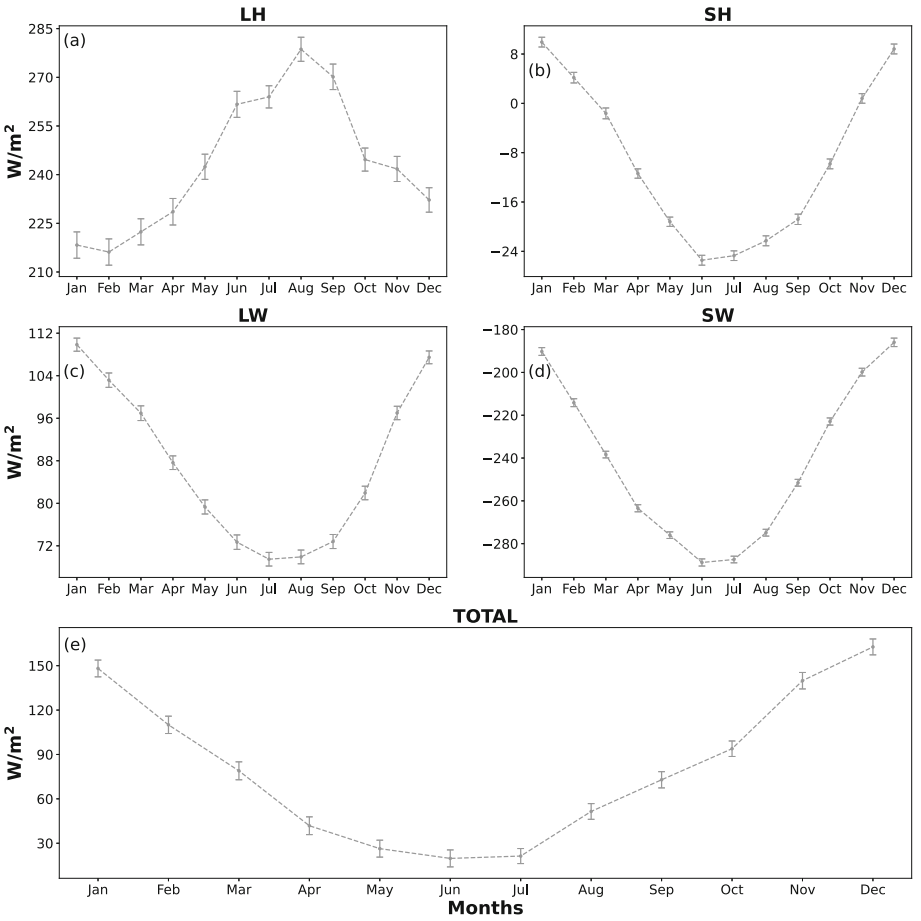


**Fig. 10** The seasonal cycle of the different heat fluxes. (a) Latent heat (LH), (b) Sensible heat (SH), (c) shortwave (SW) radiation, (d) longwave (LW) radiation, and (e) net heat flux radiation. The error bars signify the monthly standard deviation of the heat fluxes when averaged over all the years for each month

This is supported by the temperature anomaly time series that resulted in a larger warming trend in the upper water layers compared to the deeper layers. This temperature increase is also evident in the SST time series and other measures but is absent in the SAT. This finding suggests that the local atmospheric forcing may not be the primary driver underlying the water warming in the Gulf. We also calculated the heat flux budget in the Gulf and found that it is not zero, supporting the idea that the observed water warming is due to water advection from southern latitudes. The reported warming may have significant implications for the local marine ecosystem and can contribute insights to the broader understanding of the effect of remote climate change on the local marine environment.

The hypothesis of horizontal advection aligns with previous studies on the Red Sea [14;29;51;52;9]. These studies reported an increase in SST in tropical regions, ranging from around 0.014 °C $yr^{-1}$ to 0.034 °C $yr^{-1}$ since the mid-1970s, which has resulted in more frequent and severe coral bleaching and mortality, thereby raising concerns about the survival of coral reefs. The warming pattern is in accordance with the rise of the global average SST and also of

the Mediterranean Sea (Section 1). Cantin et al. [51] investigated the SST in the central Red Sea and its correlation with reef-building coral species, Diploastrea heliopora, employing three-dimensional computed tomography. From the analysis of their data combined with the Intergovernmental Panel on Climate Change (IPCC) climate model simulation, they observed a significant temperature gradient between the Gulf and the central Red Sea. They also predict that with the current warming trend, this coral species could cease growing altogether by 2070. Furthermore, an analysis (1982-2015) done by Chaidez et al. [9] on the temporal rise in SST of the Red Sea shows that the northern part warms faster than the southern part, exceeding the global rate (see Section 1).

GCM solutions of Biton et al. [52] show that the difference between the heat content of the upper 400 meters and the net surface heat flux is proportional to the heat advection from the southern region. A related study by Wolf-Vecht et al. [14] developed a one-dimensional convective model to study the structure of the water column in the Gulf. The model accurately replicates the thermal structure in the Gulf with a slight temporal lag in the summer thermocline; still, it failed to reproduce the observed salinity minimum. Introducing 40.3% advected Red Sea water rectifies the salinity discrepancy and may explain the early thermocline development due to the influx of warmer water. Berman et al. [29] used a three-dimensional coupled physical-ecological model was utilized to investigate the mechanisms driving phytoplankton blooms across the Gulf. It was observed that the surface bloom in the southern region surpassed that in the north, while the integrated bloom in the south was lower than in the north. These disparities can be attributed to spatial differences in the mixed layer depth, which is significantly deeper in the northern Gulf. Furthermore, horizontal advection was identified as a key factor regulating phytoplankton integrated biomass during the northern bloom, a factor frequently overlooked in phytoplankton bloom studies.

Another possible source of warming is shallow coastal water warming. However, if the warming of the deep water of the Gulf was solely due to the advection of warm shallow coastal water, we would expect it to be correlated with certain atmospheric conditions. In our study, we did not observe any trends in the atmospheric variables that would suggest such a correlation. We also looked for trends in other atmospheric variables such as wind speed and wind stress (see Fig. S3) and did not observe significant trends, supporting the decoupling of the ocean warming from the atmosphere conditions. Thus, we believe that the advection of warm water from southern latitudes is a more plausible explanation for the observed warming in the Gulf.

The geographical conditions of the Gulf pertain to be unique; yet, studies that analyzed CTD data of the North Aegean Sea and the Black Sea found horizontal advection to be a significant driver of the local ocean dynamics. Zodiatis et al. [53] found that the surface circulation in the North Aegean Sea is predominantly controlled by the Black Sea water current, which flows westward or southward post-Dardanelles passage. Zatsepin et al. [54] investigated an 80-90 km diameter anticyclonic eddy (during the summer and autumn of 1999), using CTD surveys, Argos-tracked drifter deployments, satellite imagery, and altimetric sea level anomaly maps. They concluded that these eddies are common in the warm season, formed due to weak macroscale circulation, and play a role in horizontal mixing of upper layer waters, deflection of the Rim Current offshore, and branching of the current around them.

Furthermore, our research findings are in harmony with the observations and conclusions presented in the IPCC report on the Red Sea, where an SST warming trend of $\sim 0.031$°C/yr since 1982-2009 and $\sim 0.07$°C/decade since 1950 [55] has been reported; these trends are close to the trend we obtained for the Gulf.

In conclusion, our comprehensive analysis of ocean temperature data in the Gulf highlights a significant rise in temperature over the entire water column. The absence of a direct correlation with local atmospheric conditions and the observation that the local net heat flux is not zero suggest that other factors, such as horizontal advection, are likely underlying the observed water warming. Our study contributes to the growing body of knowledge regarding oceanic processes and their implications for regional and global climate dynamics.

**Supplementary Information** The online version contains supplementary material available at https://doi.org/10.1007/s10584-024-03765-8.

**Acknowledgements** HG was supported by a grant from the Ministry of Science and Technology. We thank Asaph Rivlin, Modi Pilersdorf, the Israel National Monitoring Program at the Gulf of Eilat, and the Interuniversity Institute for Marine Sciences in Eilat for access to infrastructure and services.

**Funding** Open access funding provided by Ben-Gurion University. HG was supported by a grant from the Ministry of Science and Technology.

**Availability of data and materials** CTD and Meteorological data analyzed in this research work can be obtained from the website of The Israel National Monitoring Program at the Gulf of Eilat.
CTD Data - https://www.meteo-tech.co.il/EilatYam_data/ey_ctd_data_download.asp
Meteorological Data - https://www.meteo-tech.co.il/eilat-yam/eilat_en.asp.

## Declarations

**Competing Interests** The authors have no relevant financial or non-financial interests to disclose.

**Ethics approval and consent to participate** Not Applicable.

**Consent for publication** Not Applicable.



## References

1. Canadell JG, Monteiro PM, Costa MH, Da Cunha LC, Cox PM, Eliseev AV, Henson S, Ishii M, Jaccard S, Koven C et. al (2023) Global Carbon and other Biogeochemical Cycles and Feedbacks (Cambridge University Press), p 673–816
2. Bindoff NL, Stott PA, AchutaRao KM, Allen MR, Gillett N, Gutzler D, Hansingo K, Hegerl G, Hu Y, Jain S et. al (2014) Detection and Attribution of Climate Change: from Global to Regional (Cambridge University Press), p 867–952
3. Nisha P, Pranesha T, Vidya P, Ravichandran M, Murtugudde R (2024) Trend and interannual variability of the Arabian Sea heat content. J Mar Syst 242:103935
4. Xie SP (2020) Ocean warming pattern effect on global and regional climate change, AGU advances **1**(1), e2019AV000130
5. Yang YM, An SI, Wang B, Park JH (2020) A global-scale multidecadal variability driven by Atlantic multidecadal oscillation. Natl Sci Rev 7(7):1190
6. Yasunaka S, Kimoto M (2013) Upper ocean warming pattern in the past 50 years. J Oceanogr 69:87

7. Pastor F (2023) Mediterranean Centre for Environmental Studies. Mediterranean Sea surface temperature report (summer 2023), Meteorology and Climatology Area
8. Bulgin CE, Merchant CJ, Ferreira D (2020) Tendencies, variability, and persistence of sea surface temperature anomalies. Sci Rep 10(1):7986
9. Chaidez V, Dreano D, Agusti S, Duarte CM, Hoteit I (2017) Decadal trends in Red Sea maximum surface temperature. Sci Rep 7(1):8144
10. Fine M, Gildor H, Genin A (2013) A coral reef refuge in the Red Sea. Glob Change Biol 19(12):3640
11. Abir S, McGowan HA, Shaked Y, Lensky NG (2022) Identifying an evaporative thermal refugium for the preservation of coral reefs in a warming world-The Gulf of Eilat (Aqaba). J Geophys Res: Atmos **127**(24), e2022JD036845
12. Miller DR, Pfreundt U, Elifantz H, Hess WR, Berman-Frank I (2017) Microbial metatranscriptomes from the thermally stratified Gulf of Aqaba/Eilat during summer. Mar Genomics 32:23
13. Labiosa RG, Arrigo KR, Genin A, Monismith SG, van Dijken G (2003) The interplay between upwelling and deep convective mixing in determining the seasonal phytoplankton dynamics in the Gulf of Aqaba: Evidence from seawifs and modis. Limnol Oceanogr 48(6):2355
14. Wolf-Vecht A, Paldor N, Brenner S (1992) Hydrographic indications of advection/convection effects in the Gulf of Elat, Deep Sea Research Part A. Oceanographic Research Papers 39(7–8):1393
15. Reiss Z, Hottinger L (2012) The Gulf of Aqaba: Ecological Micropaleontology, vol.50 (Springer Science & Business Media)
16. Paldor N, Anati D (1979) Seasonal variations of temperature and salinity in the Gulf of Elat (Aqaba), Deep Sea Research Part A. Oceanogr Res Pap 26(6):661
17. Biton E, Silverman J, Gildor H (2008) Observations and modeling of a pulsating density current. Geophys Res Lett **35**(14), e2008GL034123
18. Abir S, McGowan HA, Shaked Y, Gildor H, Efrat M, Lensky NG (2021) Air-sea interactions in stable atmospheric conditions: Lessons from the desert semi-enclosed Gulf of Eilat (Aqaba), EGUsphere pp 1–30
19. Murray SP, Hecht A, Babcock A (1984) On the mean flow in the Tiran Strait in winter. J Mar Res 42(2):265
20. Bahartan K, Zibdah M, Ahmed Y, Israel A, Brickner I, Abelson A (2010) Macroalgae in the coral reefs of Eilat (Gulf of Aqaba, Red Sea) as a possible indicator of reef degradation. Mar Pollut Bull 60(5):759
21. Dishon G, Dubinsky Z, Fine M, Iluz D (2012) Underwater light field patterns in subtropical coastal waters: A case study from the Gulf of Eilat (Aqaba). Isr J Plant Sci 60(1–2):265
22. Genin A, Levy L, Sharon G, Raitsos DE, Diamant A (2020) Rapid onsets of warming events trigger mass mortality of coral reef fish. Proc Natl Acad Sci 117(41):25378
23. Ben-Sasson M, Brenner S, Paldor N (2009) Estimating air-sea heat fluxes in semienclosed basins: The case of the Gulf of Elat (Aqaba). J Phys Oceanogr 39(1):185
24. Genin A, Paull CK, Dillon WP (1992) Anomalous abundances of deep-sea fauna on a rocky bottom exposed to strong currents, Deep Sea Research Part A. Oceanographic Research Papers 39(2):293
25. Biton E, Gildor H (2011) The coupling between exchange flux through a strait and dynamics in a small convectively driven marginal sea: The Gulf of Aqaba (Gulf of Eilat). J Geophys Res: Oceans **116**(C6), e2011JC006944
26. Monismith SG, Genin A (2001) Tides and sea level in the Gulf of Aqaba (Eilat). J Geophys Res: Oceans **109**(C4), e2003JC002069
27. Carlson DF, Fredj E, Gildor H, Biton E, Steinbuck JV, Monismith SG, Genin A (2012) Observations of tidal currents in the northern Gulf of Eilat/Aqaba (Red Sea). J Mar Syst 102:14
28. Genin A, Lazar B, Brenner S (1995) Vertical mixing and coral death in the Red Sea following the eruption of Mount Pinatubo. Nature 377(6549):507
29. Berman H, Gildor H (2022) Phytoplankton bloom in the Gulf of Elat/Aqaba: Physical versus ecological forcing. J Geophys Res: Oceans **127**(5), e2021JC017922
30. Berman H, Gildor H, Fredj E (2023) Inter-annual variability in phytoplankton and nutrients in the Gulf of Elat/Aqaba. J Geophys Res: Oceans **128**(6), e2022JC019431
31. Carlson DF, Fredj E, Gildor H (2014) The annual cycle of vertical mixing and restratification in the Northern Gulf of Eilat/Aqaba (Red Sea) based on high temporal and vertical resolution observations. Deep Sea Res Part I 84:1
32. Wood M (2018) How sure are we? two approaches to statistical inference, arXiv preprint arXiv:1803.06214
33. Lancaster G, Iatsenko D, Pidde A, Ticcinelli V, Stefanovska A (2018) Surrogate data for hypothesis testing of physical systems. Phys Rep 748:1
34. Tibshirani RJ, Efron B (1993) An introduction to the bootstrap, Monographs on statistics and applied probability **57**(1)
35. Biton E, Gildor H (2011) Stepwise seasonal restratification and the evolution of salinity minimum in the Gulf of Aqaba (Gulf of Eilat). J Geophys Res: Oceans **116**(C8), e2011JC006944

36. Berman T, Paldor N, Brenner S (2003) The seasonality of tidal circulation in the Gulf of Elat. Israel J Earth Sci **52**(1)
37. Gulev S, Taylor PK (2000) Intercomparison and validation of ocean–atmosphere energy flux fields. final report of the Joint WCRP/SCOR Working Group on air–sea fluxes (scor working group 110)
38. Fairall CW, Bradley EF, Hare J, Grachev AA, Edson JB (2003) Bulk parameterization of air-sea fluxes: Updates and verification for the COARE algorithm. J Clim 16(4):571
39. Gill AE (1982) Atmosphere-ocean dynamics, vol. 30 (Academic press)
40. Smith SD (1988) Coefficients for sea surface wind stress, heat flux, and wind profiles as a function of wind speed and temperature. J Geophys Res: Oceans 93(C12):15467
41. Kondo J (1975) Air-sea bulk transfer coefficients in diabatic conditions. Bound-Layer Meteorol 9:91
42. Fung IY, Harrison D, Lacis AA (1984) On the variability of the net longwave radiation at the ocean surface. Rev Geophys 22(2):177
43. Josey SA, Oakley D, Pascal RW (1997) On estimating the atmospheric longwave flux at the ocean surface from ship meteorological reports. J Geophys Res: Oceans 102(C13):27961
44. Dickey T, Manov D, Weller R, Siegel D (1994) Determination of longwave heat flux at the air-sea interface using measurements from buoy platforms. J Atmos Oceanic Tech 11(4):1057
45. Berliand M, Berliand T (1952) Measurement of the effective radiation of the Earth with varying cloud amounts, Izv. Akad. Nauk SSSR, Ser. Geofiz **1**, 64
46. Sofianos S, Johns W, Murray S (2002) Heat and freshwater budgets in the Red Sea from direct observations at Bab el Mandeb. Deep Sea Res Part II 49(7–8):1323
47. Abdulla CP, Alsaafani MA, Alraddadi TM, Albarakati AM (2018) Mixed layer depth variability in the Red Sea. Ocean Sci 14(4):563
48. Berman T, Paldor N, Brenner S (2003) Annual sst cycle in the eastern Mediterranean, Red Sea and Gulf of Elat. Geophys Res Lett **30**(5), e2002GL015860
49. Joseph S, Ravichandran M, Kumar BP, Jampana RV, Han W (2017) Ocean atmosphere thermal decoupling in the eastern equatorial Indian ocean. Clim Dyn 49:575
50. Kafle HK, Bruins HJ (2009) Climatic trends in Israel 1970–2002: warmer and increasing aridity inland. Clim Change 96(1–2):63
51. Cantin NE, Cohen AL, Karnauskas KB, Tarrant AM, McCorkle DC (2010) Ocean warming slows coral growth in the central Red Sea. Sci 329(5989):322
52. Biton E, Gildor H (2011) The general circulation of the Gulf of Aqaba (Gulf of Eilat) revisited: The interplay between the exchange flow through the Straits of Tiran and surface fluxes. J Geophys Res: Oceans **116**(C8), e2010JC006860
53. Zodiatis G (1994) Advection of the black sea water in the north Aegean Sea. Global Atmos Ocean Syst 2(1):41
54. Zatsepin AG, Ginzburg AI, Kostianoy AG, Kremenetskiy VV, Krivosheya VG, Stanichny SV, Poulain PM (2003) Observations of Black Sea mesoscale eddies and associated horizontal mixing. J Geophys Res : Oceans **108**(C8), e2002JC001390
55. Hoegh-Guldberg O, Cai R, Poloczanska ES, Brewer PG, Sundby S, Hilmi K, Fabry VJ, Jung S, Skirving W, Stone DA, et. al (2014) Climate Change 2014: Impacts, Adaptation, and Vulnerability. Part B: Regional Aspects. Contribution of Working Group II to the Fifth Assessment Report of the Intergovernmental Panel on Climate Change (Cambridge University Press), chap. The Ocean, pp 1655–1731